Effective model for plasmonic coupling: A rigorous derivation

Bin Xi,* Meng Qiu,* Shiyi Xiao, Hao Xu, and Lei Zhou†

State Key Laboratory of Surface Physics and Key Laboratory of Micro and Nano Photonic Structures (Ministry of Education), Fudan University, Shanghai, 200433, China

(Received 10 March 2013; revised manuscript received 11 December 2013; published 8 January 2014)

We *rigorously* derived an effective model to describe the plasmonic couplings between nanoparticles of *general* shape. In addition to usual electric/magnetic dipolar interactions, the model also contains a radiation-correction term and an electric/magnetic cross-interacting term. The effective model was justified by full-wave simulations in different coupled plasmonic systems, for which the interplays among these terms generate fascinating behaviors. As an application of our theory, we show that the coupling strength between certain plasmonic nanoparticles can be tuned through varying the orientations of nanoparticles, leading to interesting phenomena such as ultraslow-wave plasmon propagation.

DOI: 10.1103/PhysRevB.89.035110 PACS number(s): 78.67.Pt, 78.20.Bh, 05.45.Xt

I. INTRODUCTION

Plasmonic properties of noble-metal nanoparticles (NPs) have drawn much attention recently [1–30], due to their enormous potential applications. For a single NP, the collective oscillation of its free electrons results in a localized surface plasmon (LSP) resonance at a certain frequency, determined by the size/shape of the NP and its dielectric environment. When multiple number of plasmonic NPs aggregate to form a cluster or even a lattice, couplings between neighboring NPs generate more fascinating physical phenomena, which can be utilized to realize certain practical applications. For example, couplings can lead to mode splitting of LSP resonances which is useful in sensing applications, since tunability of the LSP resonant frequency is the basis for chemical/biological sensing [1]. In addition, couplings also help transport optical signals within a deep-subwavelength scale along a plasmonic waveguide formed by an NP array, which is highly desired in integrated optics applications [2–5].

On the theoretical side, many efforts have been devoted to such problems. Brute-force simulations [6,7] are basically the numerical repeating of experiments and therefore shed little light on the inherent physics behind the discovered phenomena. While some theoretical approaches have been successfully established to compute the plasmonic couplings in NP systems based on solving complete Maxwell equations [8–11], or Maxwell equations based on the electrostatic approximation [12], these approaches are still numerical in nature and are thus inconvenient for use by nonexperts and experimentalists. For example, the coupling strengths should be recalculated when the relative configuration between two NPs is changed. Therefore, a simple effective model involving only a few parameters is very helpful for researchers with different backgrounds to understand the inherent physics in a simple way. The coupling behaviors are even more complicated and intriguing in systems containing NPs with *complex* shapes, in which optical magnetic dipole moment can be generated by the polarization currents [7]. Although electric-dipolar models were developed to describe the coupling behaviors in nanoparticles under *electrostatic* condition [13–16], they cannot be applied to study the magnetic-resonance related problems. Given a number of experiments already available on such problems but lacking simple physical explanations, we feel that a *complete* and *simple* effective model for plasmonic couplings between NPs, derived from a *rigorous* ground, is highly desired for the community.

In this paper, based on a previously established generalized tight-binding method (GTBM) for dispersive photonic media [10,31], we successfully derived (from first principles) an *analytical* model to describe the coupling behaviors in plasmonic systems containing metallic NPs of general shapes. The analytical model includes *all* interacting terms between electric and magnetic dipoles of the NPs, and its validity is well justified by full-wave simulations in various configurations. With the effective model, one can predict the rich behaviors of plasmonic couplings in complex structures without performing sophisticated computations, and can understand the inherent physics behind the complicated phenomena. For example, we found that an electromagnetic (EM) cross-interacting term in our model can lead to interesting mode-reversal behaviors in certain coupled systems. In addition, a naive consequence of the effective model is that the coupling strength can be continuously tuned from positive to negative values by simply varying the relative orientations of the NPs, leading to many interesting applications such as slow-wave plasmon transport. This effect provides an alternative and novel mechanism to realize slow-wave transport in a simple and deep-subwavelength structure, in contrast to available mechanisms employing Bragg scatterings [32] or local resonances [33].

This paper is organized as follows. After deriving the effective model in Sec. II, we justify the model by full-wave simulations under different configurations in Sec. III. Section IV contains discussions on potential applications of the model, and we conclude our paper in Sec. V.

II. THE EFFECTIVE MODEL FOR PLASMONIC COUPLING

Before presenting our analytical model, we first briefly review the GTBM which can be used to compute the coupling constant between two plasmonic NPs [10]. Consider a photonic system consisting of a collection of

*These authors equally contributed to this work.
†phzhou@fudan.edu.cn

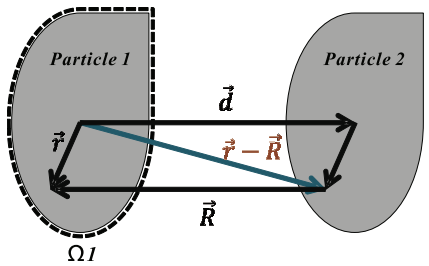

FIG. 1. (Color online) Schematic picture of the system under study.

identical metallic NPs with permittivity described by $\varepsilon_s(\omega) = \varepsilon_{\infty,s}[1 + \omega_{p,s}^2/(\omega_{e,s}^2 - \omega^2 + i\omega\Gamma)]$, embedded in a host medium with permittivity given by ε_h. Each NP is located at a position $\vec{R}_i$, and the shape of the NP can be general. The (frequency-domain) Maxwell equations of the system can be rewritten as a Schrödinger-like eigenvalue equation $\hat{\mathbf{H}}|\psi\rangle = \omega|\psi\rangle$, where the wave function is defined as $|\psi\rangle = [\vec{H} \quad \vec{E} \quad \vec{P} \quad \vec{j}]^T$ with $\{\vec{H},\vec{E},\vec{P},\vec{j}\}$ denoting magnetic field, electric field, polarization density, and polarization current density, correspondingly. The explicit form of the Hamiltonian operator $\hat{\mathbf{H}}$ can be found in Ref. 31 and our Supplemental Materials [34]. We note that a similar Hamiltonian approach has been used to study the Fano resonances in plasmonic structures [17]. According to the GTBM, rewriting the Hamiltonian as $\hat{\mathbf{H}} = \hat{\mathbf{H}}_h + \sum_{i=l}^{N}\hat{\mathbf{V}}_i$ in which $\hat{\mathbf{H}}_h$ describes the host medium and $\hat{\mathbf{V}}_i$ is the potential contributed by the ith NP (see Supplemental Materials [34] for its concrete form), we found the eigenresonance frequencies of the coupled system can be determined by solving the matrix problem

$$\det[f_0\delta_{ij} + t_{i,j} - f\delta_{ij}] = 0, \tag{1}$$

where f_0 is the (linear) eigenresonance frequency of a *single* NP obtained by solving the single-particle Schrödinger-like equation $(\hat{\mathbf{H}}_h + \hat{\mathbf{V}}_1)|\Phi(\vec{r})\rangle = 2\pi f_0|\Phi(\vec{r})\rangle$, with $\Phi(\vec{r})$ denoting the single-particle wave function. The hopping parameter is defined as

$$\begin{aligned} t_{i,j} &= \langle\varphi_i|\sum_{i\neq j}\hat{\mathbf{V}}_l|\varphi_j\rangle/(2\pi\langle\Phi|\Phi\rangle), \\ \text{with} \quad |\varphi_i\rangle &= |\Phi(\vec{r}-\vec{R}_i)\rangle, \end{aligned} \tag{2}$$

which measures the coupling strength between two NPs and can be obtained through numerical calculations once the single-particle plasmonic wave-function $\Phi(\vec{r})$ is known. Physically, $t_{i,j}$ describes the resonance-frequency change induced by coupling between the ith and the jth particle.

While such a theory can well predict the frequency splitting in coupled plasmonic systems [10], it looks complicated and the physics is hidden behind the formalisms. In what follows, we derive a simple and physically more transparent form of $t_{1,2}$ from its original expression (2). Let us consider a double-NP system as shown in Fig. 1. Put the explicit forms of $\Phi(\vec{r})$ and $\hat{\mathbf{V}}_i$ into Eq. (2), we get that

$$t_{1,2} = \frac{f_0}{2\langle\Phi \mid \Phi\rangle}\int_{\Omega 1} d\tau\{[\varepsilon_h - \varepsilon_s(\omega_0)]\vec{E}_1^*(\vec{r})\cdot\vec{E}_2(\vec{r})\}, \tag{3}$$

where the integral is performed in region Ω1 occupied by the particle 1 (see Fig. 1), $\vec{E}_1(\vec{r})$ is the $\mathbf{E}$ field component in the eigenwave function: $\varphi_1 = \Phi(\vec{r}-\vec{R}_1) = [\vec{H}_1,\vec{E}_1,\vec{P}_1,\vec{j}_1]^T$, and $\vec{E}_2(\vec{r}) = \vec{E}_1(\vec{r}-\vec{R})$ [35]. Here both $\vec{E}_1(\vec{r})$ and $\vec{E}_2(\vec{r})$ take the time-oscillation term $e^{-i\omega_0 t}$ with $(\omega_0 = 2\pi f_0)$ since they are the eigenwave functions associated with the eigenvalue f_0.

Equation (3) is remarkable since it explicitly links the frequency shift $(\sim t_{1,2})$ to the EM interacting enegry. Noting that $[\varepsilon_s(\omega_0) - \varepsilon_h]\vec{E}_1(\vec{r}) = \varepsilon_0\chi\vec{E}_1(\vec{r}) = \vec{P}_1(r)$, we can further rewrite Eq. (3) as

$$t_{1,2} = \frac{-\int_{\Omega 1}\vec{P}_1(\vec{r})\cdot\vec{E}_2(\vec{r})d\tau}{2\langle\Phi|\Phi\rangle}f_0, \tag{4}$$

which has an even clearer physical explanation. Now $\vec{E}_2(\vec{r})$ is the electric field at point $\vec{r}$ generated by the NP 2, the term $-\int_{\Omega 1}\vec{P}_1(\vec{r})\cdot\vec{E}_2(\vec{r})d\tau$ precisely represents the mutual EM interacting energy between two NPs (note the system is formed by nonmagnetic material). Meanwhile, it has been shown that the normalization constant takes the following form [10]:

$$\begin{aligned} \langle\Phi \mid \Phi\rangle = \frac{1}{2}\int d\tau\Bigg\{&\frac{\partial[\omega\varepsilon(\vec{r},\omega)]}{\partial\omega}\Bigg|_{\omega=\omega_0}|\vec{E}_1(\vec{r})|^2 \\ &+ \mu_0|\vec{H}_1(\vec{r})|^2\Bigg\}, \end{aligned} \tag{5}$$

which is just the total EM energy stored in the medium with only one NP existing [$\varepsilon(\vec{r},\omega)$ is the permittivity distribution]. Therefore, the coupling strength $t_{1,2}$ is determined by the ratio between the inter-NP interaction energy $[-\int_{\Omega 1}\vec{P}_1(\vec{r})\cdot\vec{E}_2(\vec{r})d\tau]$ and the total EM energy stored inside the whole system containing two NPs (e.g.,$2\langle\Phi|\Phi\rangle$), and $-\vec{P}_1(\vec{r})\cdot\vec{E}_2(\vec{r})$ precisely measures the relative contribution to the coupling strength at the vicinity of point $\vec{r}$. We emphasize that this formula is not just valid in *electrostatic* limit [8,13–16], but is generally true for any systems at any frequency since it is derived from the GTBM which is obtained based on the original Maxwell equations.

We can rewrite Eq. (4) to a physically more meaningful form, from which a multiple expansion technique can be easily implemented. Expressing $\vec{E}_2(\vec{r})$ with vector and scalar potentials as $\vec{E}_2 = -\nabla\varphi_2(\vec{r}) - (-i\omega_0)\vec{A}_2(\vec{r})$ and then put it to Eq. (4), we get that

$$t_{1,2} = t_{1,2}^{(E)} + t_{1,2}^{(H)}, \tag{6}$$

where

$$\begin{aligned} t_{1,2}^{(E)} &= \frac{f_0}{2\langle\Phi|\Phi\rangle}\int_{\Omega 1} d\tau\rho_{P1}^*(\vec{r})\varphi_2(\vec{r}), \\ t_{1,2}^{(H)} &= -\frac{f_0}{2\langle\Phi|\Phi\rangle}\int_{\Omega 1} d\tau\vec{j}_{P1}^*(\vec{r})\vec{A}_2(\vec{r}) \end{aligned} \tag{7}$$

represent the contributions from the charges [defined by $\rho_{P1}(\vec{r}) = -\nabla\cdot\vec{P}_1(\vec{r})$] and polarization currents [defined by $\vec{j}_{P1}(\vec{r}) = -i\omega_0\vec{P}_1(\vec{r})$] stimulated in the system, respectively. Although Eq. (6) is essentially identical to Eq. (4), the expressions presented in Eq. (7) are physically more transparent. For example, since the *effective* electric and magnetic dipole

moments carried by a NP are defined by

$$\vec{p} = \int d\tau'(\vec{r}'\rho), \quad \vec{m} = \frac{1}{2}\int [\vec{r}' \times \vec{j}_p(\vec{r}')]d\tau', \tag{8}$$

one immediately understands that all terms related to the magnetic dipole moments must come from $t_{1,2}^{(H)}$. The potential fields $\varphi_2(\vec{r})$ and $\vec{A}_2(\vec{r})$ can be further expressed as

$$\begin{aligned} \varphi_2(\vec{r}) &= \frac{1}{4\pi\varepsilon_0}\int_{\Omega 2} d\tau' \frac{\rho_{P2}(\vec{r}')\exp(ikR)}{R}, \\ \vec{A}_2(\vec{r}) &= \frac{\mu_0}{4\pi}\int_{\Omega 2} d\tau' \left[\frac{\vec{j}_{P2}(\vec{r}')\exp(ikR)}{R}\right], \end{aligned} \tag{9}$$

where ρ_{P2} and $\vec{j}_{P2}$ are the charge and polarization-current densities in NP 2 and are correlated by the charge conversion law $\nabla \cdot \vec{j}_p - i\omega_0\rho_p = 0$, $k = \omega_0/c$ is the free-space wave vector, $R = |\vec{r} - \vec{r}'|$, and the integration on $\vec{r}'$ runs over the region occupied by NP 2. Therefore, $t_{1,2}^{(E)}$, $t_{1,2}^{(H)}$ involve two integrations, which should be performed within the spatial regions occupied by two NPs, respectively. We assume that $a < d < \lambda$, in which a is the characteristic dimension of the NP, $\vec{d} = \vec{R}_2 - \vec{R}_1$ is the separation between two NPs, and λ is the wavelength. These conditions are expected to be generally valid in most situations. Therefore, we perform two multiple expansions inside the two NPs, in order to express $t_{1,2}^{(E)}$, $t_{1,2}^{(H)}$ in explicit forms of the electric and magnetic dipole moments. The derivations are quite tedious and we summarize all details in Supplemental Materials [34]. Keeping the lowest order in a/d and d/λ, we finally get

$$t_{1,2} = t_{pp} + t_{mm} + t_{pp}^{\mathrm{rad}} + t_{pm}, \tag{10}$$

where

$$t_{pp} = \frac{f_0}{2\langle\Phi|\Phi\rangle}\frac{1}{4\pi\varepsilon_0}\left[\frac{\vec{p}_1^{\,*}\cdot\vec{p}_2 - 3(\vec{p}_1^{\,*}\cdot\hat{d})(\vec{p}_2\cdot\hat{d})}{d^3}\right] \tag{11}$$

and

$$t_{mm} = \frac{f_0}{2\langle\Phi|\Phi\rangle}\frac{\mu_0}{4\pi}\left[\frac{\vec{m}_1^{\,*}\cdot\vec{m}_2 - 3(\vec{m}_1^{\,*}\cdot\hat{d})(\vec{m}_2\cdot\hat{d})}{d^3}\right] \tag{12}$$

are the usual dipolar interactions between electric (magnetic) dipoles carried by different NPs, and

$$t_{pp}^{\mathrm{rad}} = -\frac{f_0}{2\langle\Phi|\Phi\rangle}\frac{(kd)^2}{8\pi\varepsilon_0}\left[\frac{\vec{p}_1^{\,*}\cdot\vec{p}_2 + (\vec{p}_1^{\,*}\cdot\hat{d})(\vec{p}_2\cdot\hat{d})}{d^3}\right] \tag{13}$$

is the electric dipolar interaction contributed from radiation effect [noting that it carries a factor of $(kd)^2$], and

$$t_{pm} = i\frac{f_0}{2\langle\Phi|\Phi\rangle}\frac{kd}{4\pi\varepsilon_0 c}\frac{\vec{p}_1^{\,*}\cdot(\vec{m}_2\times\hat{d})}{d^3} \tag{14}$$

describes the mutual cross interaction between electric and magnetic dipoles. It should be noted that, when $\vec{p}$ and $\vec{m}$ are generated from the same charge/current distribution, a $\pi/2$ phase difference naturally exists between $\vec{p}$ and $\vec{m}$, so that t_{pm} is still a real number.

We note that $\vec{p}$, $\vec{m}$, and $\langle\Phi|\Phi\rangle$ are the only three parameters that should be calculated numerically based on the single-NP resonance. Once these three parameters are known from first-principle calculations, the couplings in general cases can be easily deduced from Eqs. (10)–(14) without doing further numerical computations. This important character not only saves lots of numerical efforts, but makes the physical picture more transparent for nonexperts and experimentalists.

Note that here we did not include the contributions from electric quadrupoles. Therefore, Eq. (10) is strictly applicable to those NPs which *only* exhibit electric and/or magnetic dipoles. However, terms related to quadrupoles can be important for NPs arranged in some particular geometries. High-order multipolar interactions can be derived in principle, although the derivations are quite complicated. We present a simple guide on how to calculate these terms in Supplemental Materials [34].

In addition, we note that Eq. (13) only contains a part of radiation corrections, which behaves like a dynamical depolarization term here. More radiation corrections, particularly the radiation damping term, can be obtained when we retain more high-order terms in expanding e^{ikR}. Again, the detailed derivations are summarized in our Supplemental Materials [34].

It is helpful to compare the strengths of those terms. Obviously, the term t_{pp}^{rad} is much smaller than t_{pp} since it carries a factor $(kd)^2$, but it can be significant when the inter-NP distance is enlarged so that the quasistatic condition does not hold anymore. However, Eq. (13) cannot work as $kd \to 1$ when the radiation is too strong and kd is no longer a small expansion parameter. Meanwhile, since the NPs are formed by *nonmagnetic plasmonic* materials, the magnetic dipole moments only come from the geometrical resonances and can be nonzero only in NPs with certain shapes [say, in structures like split ring resonator (SRR)]. Therefore, the strength of t_{mm} is hard to be compared directly with t_{pp}, since the magnitudes of $\vec{p}$ and $\vec{m}$ depend sensitively on the details of structures. We note that the EM cross-interacting term t_{pm} carries a factor (kd) in comparison with t_{pp}, which implies that it originates from radiation correction [35]. Therefore, in most cases, we have

$$t_{pp} \gg t_{pp}^{\mathrm{rad}} > t_{pm}. \tag{15}$$

It is not surprising that the leading term in Eq. (10) is just the standard electric dipole-dipole interaction t_{pp}. Such an electric dipolar interaction term has been derived from various approaches, and has been widely adopted to describe the plasmonic coupling between two nanoparticles in *electrostatic* limit [8,13–16]. In fact, in the roughest approximation, one may approximate $\vec{E}_2(\vec{r})$ in Eq. (4) as a dipolar field generated by an effective dipole moment $\vec{p}_2$ carried by NP 2. Then, the integration over $\Omega 1$ in Eq. (4) gives the effective dipole moment $\vec{p}_1$, yielding the electric dipolar interaction term t_{pp}.

Equations (10)–(15) tell us that, when the NP mainly exhibits an electric dipole moment, the dominant plasmonic coupling between two NPs will be dictated by the electric-dipolar interaction defined by Eq. (11). In the case that NPs exhibit both electric and magnetic moments, the plasmonic coupling between two NPs is very complicated and intriguing, and the EM cross interacting term t_{pm} must be considered in order to understand the coupling behaviors of NPs. The effect of dipolar magnetic coupling t_{mm} [Eq. (12)] can be singled out

only when the NP is purely magnetic (i.e., it does not exhibit a $\vec{p}$ but only exhibits a $\vec{m}$).

III. VERIFICATIONS ON THE EFFECTIVE MODEL

In what follows, we perform extensive full-wave simulations on particular plasmonic coupled systems to verify the effective model presented in Eq. (10).

A. Electric dipolar interaction

In a system containing two identical NPs which exhibit only electric dipoles, Eq. (10) contains only t_{pp} and t_{pp}^{rad}. In quasistatic limit with $kd \to 0$, we can drop the t_{pp}^{rad} term and Eq. (10) can be rewritten as

$$t_{1,2} \approx \frac{f_0}{8\pi\varepsilon_0\langle\Phi|\Phi\rangle}\frac{(1-3\cos^2\theta)|\vec{p}|^2}{d^3}, \tag{16}$$

where $\vec{p}_1 = \vec{p}_2 = \vec{p}$ denotes the electric dipole moment carried by the two identical NPs, and θ is the angle between the two vectors $\vec{p}$ and $\vec{d}$. Equation (16) shows that the coupling are determined by two important parameters d and θ.

We performed full-wave simulations on a particular system to verify Eq. (16). As shown in Fig. 2(b), the system contains two identical gold NPs in ellipsoidal shapes (with semimajor $a = 8$ nm and semiminor $b = 4$ nm), separated by a distance d. We note that NPs of this size can be fabricated experimentally [36,37], and the ellipsoidal shape is adopted here only for convenience. In fact, we found similar results with NPs taking other shapes. Due to its anisotropic shape, such an NP exhibits two plasmonic resonances and we are primarily interested in the fundamental mode (with dipole moment polarized along the long axis). In our finite-difference-time-domain (FDTD) simulations [38] we assumed $\mu_s = \mu_0$ and employed a Drude model to describe the dielectric response of Au with parameters given by $\varepsilon_{\infty,s} = 9\varepsilon_0$ $\omega_{p,s} = [2\pi(\varepsilon_{\infty,s}/\varepsilon_0)^{-1/2}] \times 2176.2$ THz. To highlight the physics only, we neglected the loss everywhere. We first put a single NP into a fictitious rectangle waveguide formed by two perfect-electric-conductor (PEC) walls (parallel to the yz plane) and two perfect-magnetic-conductor (PMC) walls (parallel to the xz plane). The transverse-electromagnetic (TEM) mode of such a waveguide can well mimic a plane wave polarized with $\vec{E}||\hat{x}$ [see middle panel of Fig. 2(b)], so that the calculated transmission/reflection spectrum precisely describes the response of a single NP with respect to a plane wave excitation. The plasmonic resonance frequency f_0 of a single NP can be clearly identified from the peak of the reflection spectrum [black solid line in Fig. 2(a)]. When another NP is added to form a dimer, the inter-NP interaction splits the original resonance into two modes, corresponding to symmetrically and antisymmetrically coupled modes (with dipole moments in two NPs parallel or antiparallel with each other, sometimes called "bright" and "dark" modes), with resonance frequencies denoted by f_+ and f_-, respectively. According to the GTBM, two eigenfrequencies are given by $f_\pm = f_0 + t_{1,1} \pm t_{1,2}$ in which $t_{1,1}$ is the onsite hoping term [10]. Therefore, the frequency *splitting* $\Delta f = f_+ - f_- = 2t_{1,2}$ precisely measures the coupling strength $t_{1,2}$. We note that such a relationship was also derived by other authors [14–16].

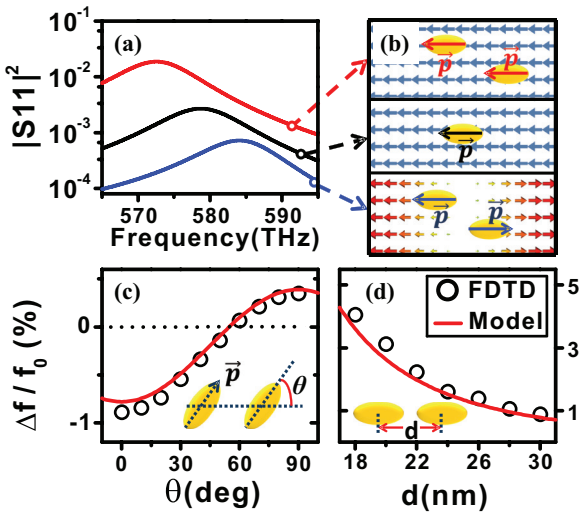

FIG. 2. (Color online) (a) Computed reflection spectra of a single NP under the TEM excitation (black line) and the coupled system under the TEM (red line) and TM10 (blue line) excitations. (b) Schemes of probing the plasmonic resonance of a single NP and the bright/dark modes of a coupled system. (c) Calculated frequency splitting versus θ with d fixed as 30 nm and (d) versus d with θ fixed as 0°, for the coupled-NP system, obtained by FDTD simulations (open circles) and the effective model (solid lines).

To identify these two modes, we put the dimer into the fictitious waveguide and study the reflection spectra with respect to different excitation modes [see Fig. 2(b)]. The calculated spectrum with respect to a TEM-mode excitation [red line in Fig. 2(a)] exhibits a pronounced peak, which can be easily identified as the bright mode by examining the current distributions in two NPs. However, the dark mode cannot be identified from such a calculation, since it has an extremely small response to the plane wave excitation. To solve this problem, we purposely excite the TM10 waveguide mode in which the **E** field exhibits opposite directions at the centers of two NPs, as shown in the bottom panel of Fig. 2(b). Such an excitation field has the largest overlapping integral with the dark mode but has a zero overlapping integral with the bright mode. As the result, the peak in such a calculated reflection spectrum precisely determines the dark mode position f_- [see the blue line in Fig. 2(a)].

Therefore, through varying the positions of these two NPs, we can study how the coupling constant $t_{1,2}$ depends on $\vec{d}$ by numerically estimating the frequency splitting Δf under different configurations. Open circles in Figs. 2(c) and 2(d) depict the FDTD simulated Δf (and thus $t_{1,2}$) as a function of the polarization angle θ with d fixed as 30 nm, and as a function of d with θ fixed as 0°, respectively. As a comparison, we computed the $\Delta f \sim \theta$ and $\Delta f \sim d$ relations based on the effective model as shown in Eq. (16) under the conditions specified above, and depicted the corresponding curves in Figs. 2(c) and 2(d) as solid lines. Here both the dipole moment $\vec{p}$ and the normalization constant $\langle\Phi|\Phi\rangle$ are obtained by *first-principle* calculations on the realistic system using a finite-element method (FEM) [39], so that the solid curves

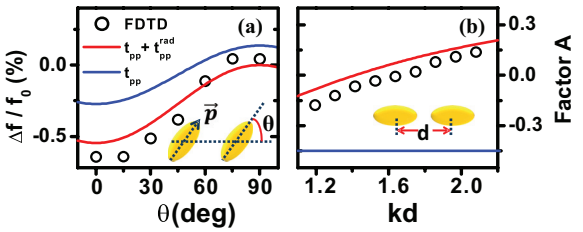

FIG. 3. (Color online) (a) Calculated frequency splitting versus θ with $(kd)^2$ fixed as 2 and (b) factor A versus kd, for the coupled-NP system, obtained by FDTD simulations (open circles) and the effective model (solid lines).

are obtained *without any adjustable parameters*. We note that the FDTD results agree very well with formula Eq. (16) in both cases, which justifies the effective model for plasmonic coupling in electric-coupling case.

B. Electric radiation correction

Previous discussions are strictly valid only in the quasistatic limit. As the inter-NP distance d is increased, the term t_{pp}^{rad} becomes more and more important and thus cannot be dropped. In such cases, the effective model becomes

$$t_{1,2} \approx \frac{f_0|\vec{p}|^2}{8\pi\varepsilon_0\langle\Phi|\Phi\rangle d^3}\left[\left(1-\frac{(kd)^2}{2}\right)-\left(3+\frac{(kd)^2}{2}\right)\cos^2\theta\right]. \tag{17}$$

We note that the radiation correction dramatically changes the angular dependence of the coupling strength. To quantify such an effect, let us define a factor A as

$$A=\frac{\Delta f(\theta=90^\circ)}{\Delta f(\theta=0^\circ)}=-\frac{1}{2}+\frac{(kd)^2}{2+(kd)^2}, \tag{18}$$

which is exactly -0.5 in the quasistatic limit. The deviation from this value thus measures the contribution of the radiation correction.

To justify the radiation-corrected model (17), we studied NPs with larger sizes (with $a = 40$ nm and $b = 20$ nm) and larger inter-NP distance d, based on the same simulation techniques presented in last subsection. With d fixed as 150 nm, we depicted in Fig. 3(a) the calculated relative frequency splitting $\Delta f/f_0$ as a function of polarization angle θ as open circles. It is clear that a single dipolar interaction term t_{pp} cannot reasonably describe the angular dependence of the coupling strength, while adding the radiation correction term t_{pp}^{rad} significantly improves the consistency between the model and simulation results. To further highlight the role of radiation correction, we computed the factor A in coupled double-NP systems with different d values. Figure 3(b) shows that the A factor significantly deviates from the quasistatic value -0.5 in large d cases. With term t_{pp}^{rad} included, the model can quantitatively account for such a deviation, highlighting the role of the radiation correction. Again, all parameters involved in our effective model are not adjustable parameters, but rather determined by first-principles calculations.

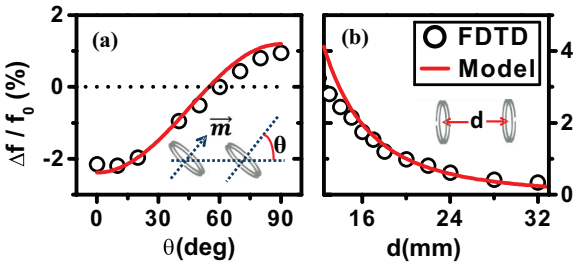

FIG. 4. (Color online) (a) Calculated frequency splitting versus θ with d fixed as 15 mm and (b) versus d with θ fixed as 0°, for the coupled system consisting of two BC-SRRs, obtained by FDTD simulations (open circles) and the effective model (solid lines). The BC-SRR structures were assumed to be formed by PEC.

C. Magnetic dipolar interaction

We turn to justify the "magnetic" part of the effective model for plasmonic coupling. As mentioned in last section, the effective model becomes extremely complicated when the NP exhibits both $\vec{p}$ and $\vec{m}$ [7]. To make things easier, here we purposely designed a NP to exhibit $\vec{m}$ only (with $\vec{p}=0$), so that the interaction between two such NPs should only contain the term t_{mm}. In this case, Eq. (12) can be rewritten as

$$t_{1,2} \approx \frac{f_0\mu_0}{8\pi\langle\Phi|\Phi\rangle}\frac{(1-3\cos^2\theta)|\vec{m}|^2}{d^3}, \tag{19}$$

where $\vec{m}_1=\vec{m}_2=\vec{m}$ denotes the magnetic dipole moment carried by each NP, and θ is now the angle between $\vec{m}$ and $\vec{d}$. We chose the broadside-coupled SRR (BC-SRR) structure as our NP, which was shown to exhibit a *pure* magnetic dipole moment (with zero electric dipole moment) at its lowest resonance mode [40]. Noting that the derived effective model is valid in *any frequency domain* since we did not specify frequencies in deriving the model, here we chose the microwave regime to justify Eq. (19) where the involved computations are relatively less time consuming. However, we emphasize that similar results can be obtained in higher frequencies. As shown in the inset to Fig. 4, the system we studied contains two BC-SRRs (each with radius $r = 4.4$ mm, inter-ring distance $s = 0.7$ mm, metal linewidth $b = 0.8$ mm, and gap size $l = 1$ mm), separated by a distance d. The coupling between these two BC-SRRs generates two coupled magnetic modes, each of which can be probed by a particular waveguide mode excitation. Following the similar approach as the electric-coupling case, we performed extensive FDTD simulations [38] to compute the frequency splitting $\Delta f = f_+ - f_- = 2t_{1,2}$ for the coupled system under different configurations. Open circles in Fig. 4 depict the FDTD calculated frequency splitting Δf versus d and θ, respectively, which can again be very well described the effective model Eq. (19) (solid lines in Fig. 4), obtained without any adjustable parameters. Such an excellent agreement is remarkable, since here all involved parameters are derived from *first principles* (by FEM simulations [39]) without any fitting procedures.

D. EM cross-interacting term

We now discuss the term t_{pm} in Eq. (10), which describes the interaction between the electric dipole of one NP with the

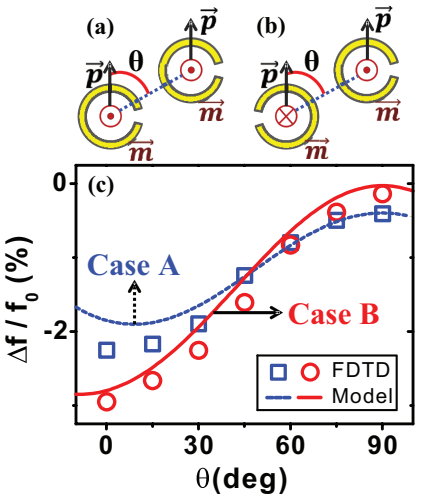

FIG. 5. (Color online) Structures of the single ring coupling system in case (a) the two rings split to the same direction and (b) two rings split to opposite directions. And (c) calculated frequency splitting versus θ with d fixed as 15 mm, for the coupled system consisting of two SRRs, obtained by FDTD simulations (symbols) and the effective model (lines). Blue line and symbols are for the SRRs split to the same direction and red ones for the SRRs split to the opposite directions. The SRR structures were assumed to be formed by PEC.

magnetic dipole of another NP. Such an EM cross-interacting term has not been adequately noted in previous studies, but here we demonstrate that it plays a significant role in understanding the fascinating coupling behaviors in NPs with complex structures.

We choose a single SRR (with $r = 4.4$ mm, $b = 0.8$ mm, and $l = 1$ mm) as our NP to illustrate this problem, since such a structure exhibits both $\vec{p}$ and $\vec{m}$ at its lowest resonance and has been most widely studied in the past 10 years [12,18,40,41,42]. The most interesting property of such a NP is that the direction of $\vec{m}$ induced on it *sensitively* depends on the position of split. As shown in Figs. 5(a) and 5(b), we place two such SRRs on the same plane, and study the coupling behaviors of the coupled system in two cases where the two splits are on the same sides of the SRRs (case A) or on opposite sides (case B). The directions of induced $\vec{p}$ and $\vec{m}$ have been explicitly indicated in the figure in two cases. If we only consider the two dipolar interactions, we got that

$$t_{pp} + t_{mm} \propto (1 - 3\cos^2\theta)\frac{|\vec{p}|^2}{\varepsilon_0}\begin{cases} +\mu_0|\vec{m}|^2 & \text{case A} \\ -\mu_0|\vec{m}|^2 & \text{case B} \end{cases}. \quad (20)$$

Equation (20) indicates that the $\Delta f \sim \theta$ relations in two cases should be two parallel curves, which can never intersect with each other. We performed extensive FDTD simulations [38] to compute the frequency splitting in the two cases, and depicted the two computed $\Delta f \sim \theta$ relations in Fig. 5(c) as open circles. We found that the two FDTD-computed $\Delta f \sim \theta$ curves exhibit a clear intersection point at $\theta \sim 60^\circ$, evidencing very interesting mode sequence reversal effect.

Such interesting coupling behaviors can be fully understood by our effective model with all terms included, in particular, the EM cross-interacting term. For the two configurations studied here, we can rewrite the *full* effective model explicitly as

$$t_{1,2} \approx \frac{f_0}{8\pi\langle\Phi|\Phi\rangle d^3}\left\{\frac{|\vec{p}|^2}{\varepsilon_0}\left[\left(1 - \frac{(kd)^2}{2}\right) - \left(3 + \frac{(kd)^2}{2}\right)\cos^2\theta\right] \pm \mu_0|\vec{m}|^2 \mp \frac{\omega_0|\vec{p}||\vec{m}|d}{\varepsilon_0 c^2}\sin\theta\right\} \quad (21)$$

in which the upper (lower) sign in front of the last two terms is for case A (B). Most importantly, we found that the term t_{pm} exhibits a completely different angle dependence ($\sim \sin\theta$) compared with other terms, and their competitions can change the angle dependence of the coupling strength. As a direct proof, we employed the full model (with every involved parameters obtained by *first-principles* calculations) to calculate the $\Delta f/f_0 \sim \theta$ curves in both configurations, and depicted the results as solid lines in Fig. 5(c). Remarkable agreements between the model and FDTD results are noted. In particular, the full model directly reproduced the intersection phenomenon at the angle when $t_{mm} = -t_{pm}$, demonstrating that such a mode reversal phenomenon is caused by the interplay between different terms in the effective model. Note that here we only considered one particular geometry, but already very interesting phenomena were discovered. One may easily expect more fascinating coupling behaviors in more complicated cases, which remain to be explored. In fact, a similar mode-sequence reversal effect was already discovered in coupled SRR systems, although in different configurations [12,18].

IV. APPLICATIONS OF THE EFFECTIVE MODEL

The effective model can help us understand the coupling behaviors without performing complicated computations. For example, Eq. (16) and Fig. 2 already show that the coupling between two NPs is highly sensitive to the polarization angle θ, and can even approach to zero in a particular case. This highly nontrivial effect can lead to many interesting predictions, such as ultraslow-wave plasmon transport in a carefully designed plasmonic waveguide. To see how it happens, we performed full-wave numerical simulations based on FEM [39] to study

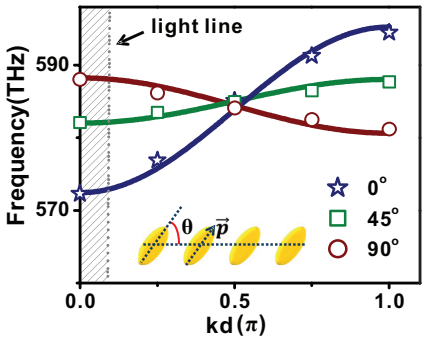

FIG. 6. (Color online) Dispersion relations of plasmon transport for three chains of nanoellipsoids oriented at different angles, obtained by FEM calculations (scatters) and the GTBM (lines). The nanoellipsoid is the same as that in Fig. 2. The distance between two adjacent nanoellipsoids is $d = 24$ nm.

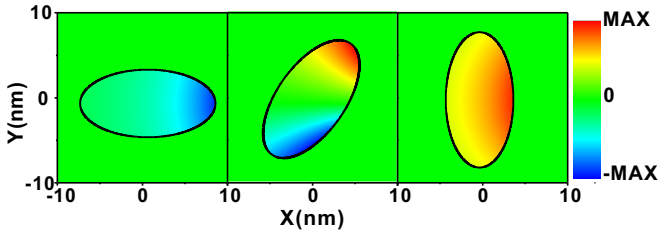

FIG. 7. (Color online) Distributions of coupling strength density $[-\vec{P}_1(\vec{r}) \cdot \vec{E}_2(\vec{r})]$ on the x-y plane of NP 1 in coupled NP systems, with NPs oriented along angles (a) $\theta = 0^\circ$, (b) $\theta = 54.7^\circ$, and (c) $\theta = 90^\circ$, calculated by the FEM [39]. The dimension of each nanoellipsoid and inter-NP distance is the same as in Fig. 6.

the dispersion of plasmon transport in a periodic chain of Au nanoellipsoids orientated at angle θ with respect to the chain direction, as shown in the inset to Fig. 6. Symbols in Fig. 6 depict the calculated $f \sim k$ dispersion relations (with k denoting the Bloch wave vector) for θ taking different values. In comparison, lines in the same figure represent the dispersion relation calculated by the GTBM formula [by solving Eq. (1)] imposing Bloch boundary condition

$$f = f_0 + 2t_{1,1} + 2t_{1,2}\cos(kd). \tag{22}$$

Here the parameter $f_0 = 578.7$ is calculated by the FEM for a single NP, $t_{1,1} = -1.882, t_{1,2} = -5.639$ for $\theta = 0^\circ$, $t_{1,1} = -0.643, t_{1,2} = -0.740$ for $\theta = 45^\circ$, and $t_{1,1} = -0.214, t_{1,2} = 1.962$ for $\theta = 90^\circ$ are obtained by FEM calculations based on Eq. (2). The units of parameters f_0, $t_{1,2}$, $t_{1,1}$ are all THz. We note that the FEM results are in excellent agreement with the GTBM results. Moreover, both of them show that the slope of the dispersion changes from a positive value to a negative value as θ increases from 0° to 90°, which is consistent with the prediction of the effective model (16) as well as Fig. 2(c). The most striking prediction of the effective model is that the $t_{1,2}$ becomes exactly zero at $\theta = \cos^{-1}(1/\sqrt{3}) \sim 54.7^\circ$, indicating that the plasmon transport becomes completely dispersionless and the transport velocity is exactly zero in such a case. Indeed, the FEM calculated dispersion for $\theta = 45^\circ$ already shows that the dispersion is very weak, which is a side evidence for the above discussions [43].

It is interesting to explore the intrinsic physics underlying such an unusual zero-coupling effect. Equation (4) shows that the interaction between two NPs should be *nonzero locally* whenever the field is nonzero, but why the coupling strength can be exactly zero in some case? We found that this is because those local contributions in different spatial regions of the NPs can cancel each other in some situations, leading to a global zero-coupling effect. To quantify this argument, we depicted in Fig. 7 the distribution of local contribution to the coupling strength, defined by $-\vec{P}_1(\vec{r}) \cdot \vec{E}_2(\vec{r})$ for the position $\vec{r}$ (inside NP 1), on the center-symmetrical x-y planes of the NPs with different polarization angles. In both $\theta = 0^\circ$ and $\theta = 90^\circ$ cases, the local contributions inside the NP are in-phase, but the signs of these contributions are different so that the final inter-NP coupling is positive (negative) in the case of $\theta = 0^\circ$ ($\theta = 90^\circ$). The most intriguing thing is the $\theta = 54.7^\circ$ case where the local contributions in different regions exhibit different signs, so that they exactly cancel each other, leading to a zero coupling constant.

We note that there are already several mechanisms discussed in literature that can lead to slow wave transport, such as using Bragg scatterings to engineer the dispersion in a photonic crystal [32] and using Fano-like resonances to engineer the group refraction index in a carefully designed photonic system [33]. The presently proposed mechanism, based on the cancellations of local coupling contributions, differs obviously from previously established ones [32,33]. Compared to those previous schemes [32,33], our mechanism does not request perfect periodic spatial ordering of the structure, and the system is very simple and has a deep-subwavelength size. All of these characters are favorable in practical applications.

As a final remark, we note that here we only considered the simplest case where the radiation corrections can be dropped so that the zero-coupling effect is found at $\theta = 54.7^\circ$. Such a prediction can also be obtained by a simple dipolar model without using our full model. However, in general situations where the radiation corrections and the magnetic contributions exist, the zero-coupling angle can be very different from this value and can only be obtained based on our full effective model Eq. (10). We further note that a previous experiment has already demonstrated that the coupling strength between two NPs can be controlled by varying the orientation angle of one of the NPs [19,20]. Although preformed on a configuration different from our case, such an experiment still clearly shows that the predictions discussed in this section can in principle be demonstrated. We are looking forward to such experiments.

V. CONCLUSIONS

In summary, we have derived from first principles an effective model to describe the coupling behaviors in general plasmonic systems. The effective mode contains not only the usual electric and magnetic dipolar interactions, but also a radiation correction term as well as an EM cross-interacting term. The model is well justified by full-wave simulations in different situations, and predicts several fascinating coupling phenomena. In particular, we show that the EM cross interacting term can lead to an intriguing mode sequence reversal effect and interparticle plasmonic coupling can be exactly zero at certain conditions. Many more fascinating applications and predictions of our model can be expected and we are looking forward to experimental verifications on the effective model. We believe that extending our theory to study other related physical problems in nanoplasmonics (such as the Fano resonances [17]) is highly interesting.

ACKNOWLEDGMENTS

This work was supported by the NSFC (No. 60990321, No. 11174055), Program of Shanghai Subject Chief Scientist (12XD1400700), and MOE of China (No. B06011).

[1] M. Rycenga, C. M. Cobley, J. Zeng, W. Li, C. H. Moran, Q. Zhang, D. Qin, and Y. Xia, Chem. Rev. **111**, 3669 (2011).

[2] N. J. Halas, S. Lal, W.-S. Chang, S. Link, and P. Nordlander, Chem. Rev. **111**, 3913 (2011).

[3] E. Ozbay, Science **311**, 189 (2006).

[4] S. A. Maier, P. G. Kik, H. A. Atwater, S. Meltzer, E. Harel, B. E. Koel, and A. A. G. Requicha, Nat. Mater. **2**, 229 (2003).

[5] N. L. Rosi and C. A. Mirkin, Chem. Rev. **105**, 1547 (2005).

[6] J. Zhou, T. Koschny, M. Kafesaki, and C. M. Soukoulis, Phys. Rev. B **80**, 035109 (2009).

[7] N. Liu, H. Liu, S. Zhu, and H. Giessen, Nat. Photon. **3**, 157 (2009).

[8] I. D. Mayergoyz, D. R. Fredkin, and Z. Zhang, Phys. Rev. B **72**, 155412 (2005).

[9] U. Hohenester and J. Krenn, Phys. Rev. B **72**, 195429 (2005).

[10] B. Xi, H. Xu, S. Xiao, and L. Zhou, Phys. Rev. B **83**, 165115 (2011).

[11] R.-L. Chern, X.-X. Liu, and C.-C. Chang, Phys. Rev. E **76**, 016609 (2007).

[12] D. A. Powell, M. Lapine, M. V. Gorkunov, I. V. Shadrivov, and Y. S. Kivshar1, Phys. Rev. B **82**, 155128 (2010).

[13] T. J. Davis, K. C. Vernon, and D. E. Gómez, Phys. Rev. B **79**, 155423 (2009).

[14] T. J. Davis, D. E. Gómez, and K. C. Vernon, Nano Lett. **10**, 2618 (2010).

[15] T. J. Davis, M. Hentschel, N. Liu, and H. Giessen, ACS Nano **6**, 1291 (2012).

[16] F. Eftekhari and T. J. Davis, Phys. Rev. B **86**, 075428 (2012).

[17] B. Gallinet and O. J. F. Martin, Phys. Rev. B **83**, 235427 (2011).

[18] D. A. Powell, K. Hannam, I. V. Shadrivov, and Y. S. Kivshar, Phys. Rev. B **83**, 235420 (2011).

[19] A. M. Funston, C. Novo, T. J. Davis, and P. Mulvaney, Nano Lett. **9**, 1651 (2009).

[20] C. Tabor, D. Van Haute, and M. A. El-Sayed, ACS Nano **3**, 3670 (2009).

[21] S.-C. Yang, H. Kobori, C.-L. He, M.-H. Lin, H.-Y. Chen, C. Li, M. Kanehara, T. Teranishi, and S. Gwo, Nano Lett. **10**, 632 (2010).

[22] K. D. Ko, A. Kumar, K. H. Fung, R. Ambekar, G. L. Liu, N. X. Fang, and K. C. Toussaint, Jr. Nano Lett. **11**, 61 (2011).

[23] M. J. Guffey and N. F. Scherer, Nano Lett. **10**, 4302 (2010).

[24] V. Myroshnychenko, J. Rodriguez-Fernandez, I. Pastoriza-Santos, A. M. Funston, C. Novo, P. Mulvaney, L. M. Liz-Marzan, A. de Garcia, and F. Javier, Chem. Soc. Rev. **37**, 1792 (2008).

[25] J. Zuloaga, E. Prodan, and P. Nordlander, Nano Lett. **9**, 887 (2009).

[26] J. Zuloaga and P. Nordlander, Nano Lett. **11**, 1280 (2011).

[27] P. Nordlander, C. Oubre, E. Prodan, K. Li, and M. I. Stockman, Nano Lett. **4**, 899 (2004).

[28] M. L. Brongersma, J. W. Hartman, and H. A. Atwater, Phys. Rev. B **62**, R16356 (2000).

[29] M. W. Chu, V. Myroshnychenko, C. H. Chen, J. P. Deng, C. Y. Mou, and F. J. G Abajo, Nano Lett. **9**, 399 (2009).

[30] K. H. Su, Q. H. Wei, X. Zhang, J. J. Mock, D. R. Smith, and S. Schultz, Nano Lett. **3**, 1087 (2003).

[31] H. Xu, Q. He, S. Xiao, B. Xi, J. Hao, and L. Zhou, J. Appl. Phys. **109**, 023103 (2011).

[32] T. Baba, Nat. Photon. **2**, 465 (2008).

[33] N. Papasimakis and N. I. Zheludev, Opt. Photon. News **20**, 22 (2009).

[34] See Supplemental Material at http://link.aps.org/supplemental/10.1103/PhysRevB.89.035110 for derivations of Eqs. (3), (10)-(14), and a simple guide to derive the high-order multipole interaction terms and high-order radiation corrections in the effective model.

[35] A. Raman and S. Fan, Phys. Rev. Lett. **104**, 087401 (2010).

[36] B. Ding, Z. Deng, H. Yan, S. Cabrini, R. N. Zuckermann, and J. Bokor, J. Am. Chem. Soc. **132**, 3248 (2010).

[37] Y.-T. Yu and P. Dutta, Sensors Actuators B: Chem. **157**, 444 (2011).

[38] CONCERTO 7.0, Vector Fields Limited, England (2008).

[39] COMSOL Multi-physics 3.5, developed by COMSOL ©, network license (2008).

[40] L. Zhou, X. Huang, Y. Zhang, and S.-T. Chui, Mater. Today **12**, 52 (2009).

[41] J. B. Pendry, A. J. Holden, D. J. Robbins, and W. J. Stewart, Microwave Theory Tech. **47**, 2075 (1999).

[42] J. Zhou, Th. Koschny, M. Kafesaki, E. N. Economou, J. B. Pendry, and C. M. Soukoulis, Phys. Rev. Lett. **95**, 223902 (2005).

[43] We cannot directly study the dispersion in the $\theta = 54.7^\circ$ case due to the convergence problems in computations.